IEEE Access
Multidisciplinary | Rapid Review | Open Access Journal

Received March 19, 2019, accepted April 15, 2019, date of publication April 30, 2019, date of current version May 14, 2019.

Digital Object Identifier 10.1109/ACCESS.2019.2913985

Synchronous LoRa Mesh Network to Monitor Processes in Underground Infrastructure

CHRISTIAN EBI[1], (Member, IEEE), FABIAN SCHALTEGGER[2], ANDREAS RÜST[2], (Member, IEEE), AND FRANK BLUMENSAAT[1,3]

[1]Swiss Federal Institute of Aquatic Science and Technology (Eawag), 8600 Dübendorf, Switzerland
[2]Institute of Embedded Systems, Zurich University of Applied Sciences (ZHAW), 8401 Winterthur, Switzerland
[3]Institute of Environmental Engineering, ETH Zurich, 8093 Zurich, Switzerland

Corresponding author: Frank Blumensaat (frank.blumensaat@eawag.ch)

ABSTRACT Collecting precise real-time information on urban drainage system performance is essential to identify, predict, and manage critical loading situations, such as urban flash floods and sewer overflows. Although emerging low-power wireless communication techniques allow efficient data transfers with great above-ground performance, for underground or indoor applications in a large coverage range are difficult to achieve due to physical and topological limitations, particularly in dense urban areas. In this paper, we first discuss the range limitations of the LoRaWAN standard based on a systematic evaluation of a long-term operation of a sensor network monitoring in-sewer process dynamics. Analyses reveal an–on average–five-fold higher data packet loss for sub-surface nodes, which steadily grows with increasing distance to the gateway. Second, we present a novel LPWAN concept based on the LoRa® technology that enhances transmission reliability, efficiency, and flexibility in range-critical situations through meshed multi-hop routing and ensures a precise time-synchronization through optional GPS or DCF77 long-wave time signaling. Third, we illustrate the usefulness of the newly developed concept by evaluating the radio transmission performance for two independent full-scale field tests. Test results show that the synchronous LoRa mesh network approach clearly outperforms the standard LoRaWAN technique with regard to the reliability of packet delivery when transmitting from range-critical locations. Hence, the approach is expected to generally ease data collection from difficult-to-access locations such as underground areas.

INDEX TERMS Environmental engineering, Internet of Things, LoRaWAN, mesh networks, time-division multiple access, water pollution, wide area networks, wireless sensor networks, urban drainage.

I. INTRODUCTION

Due to the miniaturization of hardware components, increasing computational capacities, and an ubiquitous integration of various types of technology in our everyday life promise a plethora of data in the near future. This process - often referred to as the digital transformation – is expected to also affect the field of urban water management [1], [2]. Collecting spatially distributed, real-time information within water supply and wastewater collection networks is essential to provide a reliable service and to identify, predict and manage critical situations. In the context of urban drainage management, this data collection helps to address a variety of aspects, including: estimation of the precise location and quantity of sewer infiltration, early detection of potential sewer blockages, prediction of urban flash floods, and mitigation of river water pollution through coordinated overflow control. Moreover, flexible low-cost monitoring techniques are becoming increasingly relevant amid a growing number of decentralized stormwater treatment facilities and the need to monitor their performance.

Still, it remains a challenge to reliably monitor sewer system dynamics underground and at an adequate spatial density and temporal resolution. Unlike above-ground applications, sensor and data transmission technology implemented in sewer networks must fulfill specific requirements. The equipment needs to be robust to withstand unfavorable, aggressive conditions; sensing and data transmission should consume a minimum amount of energy to allow long-lasting battery cycles and still provide recordings at a

The associate editor coordinating the review of this manuscript and approving it for publication was Nick Harris.

sufficient temporal resolution (minutes); remote operation monitoring and non-invasive data transmission is desirable to reduce service intervals at difficult-to-access locations; the equipment design requires compliance with explosion-proof standards (e.g. the ATEX directive); and underground radio transmissions must tolerate significantly higher signal attenuation [3].

While recent technological developments have improved the transmission efficiency of above-ground applications [4], data collection techniques in areas of imperfect radio coverage have not seen the same development progress, and thus are often very limited [5], [6]. Attempts to overcome these constraints include the use of memory cards, wired communication, and off-the-shelf radio technology. Memory cards have sufficient capacity to log sensor readings over long periods but do not allow for remote monitoring. Wired communication requires in-situ cable infrastructure, but is difficult to maintain and costly to deploy. Standard cellular radio technology allows for limited wireless data transmission (e.g. due to high signal attenuation), but hardware, installation, and energy consumption are also costly.

Low-Power Wide Area Network (LPWAN) systems such as LoRaWAN, SigFox, Ingenu, Weightless-P and NarrowBand-IoT (NB-IoT) aim to overcome these challenges [4]. However, comparing the different technologies is difficult in a rapidly advancing and highly competitive market. Bardyn *et al.* [7] attempt such an evaluation and provide an overview of LPWAN techniques in Europe, comparing main technologies and solutions at the time.

After evaluating several characteristics of these systems, including transmission capacity, range, energy efficiency, security, device integration, state of development, open vs. proprietary technology we find that advantages and disadvantages often balance out. While all devices have long-range capabilities and a high energy efficiency, individual key features would make them a preferred solution for a specific problem. LoRaWAN [8] appears particularly suitable for scientific applications due to i) the open protocol, ii) the availability and low cost of hardware components, and iii) the possibility to establish small, stand-alone private networks on unlicensed frequency bands (US: 902-928 MHz, EU: 863-870 MHz).

In this study, we demonstrate how recent LPWAN technology can be further engineered to fit the particular purpose of distributed monitoring, in urban drainage networks and beyond. The main contributions of this paper are to:

1) Discuss existing LPWAN techniques with a focus on highly scalable solutions for process monitoring in underground infrastructure;
2) Evaluate the long-term performance of a large full-scale LoRaWAN sensor network (own work) and highlight transmission limitations of the LoRaWAN standard for deep underground applications;
3) Introduce a novel LPWAN concept that is based on the physical LoRa layer to overcome these constraints; and
4) Provide evidence of the superiority of the new technique compared to the LoRaWAN standard using two independent full-scale field tests.

II. RELATED WORK

Various large-scale LPWAN monitoring initiatives have been reported, e.g., for river flow monitoring (https://flood.network/), smart water grid management [9], coastal flood forecasting [10], air pollution monitoring [http://carbosense.wikidot.com/]. While different techniques can be used for long-range data transmission, the LoRaWAN standard is most frequently applied. LoRaWAN is a standardized wireless radio network protocol based on the LoRa technology, a low power, spread-spectrum modulated and high sensitivity radio system [11]. The communication range stretches from a few kilometers in urban areas [12] up to several kilometers under line-of-sight or open area conditions [13].

LoRaWANs form star-type network topologies and allow single wireless hop communication between end-devices and a central gateway. Data transmission is organized through the very sparse ALOHA random access. While the transmission efficiency of ALOHA is high under ideal conditions, which include sufficient signal strength (RSSI), line-of-sight, low spreading factor (SF), and short on-air time, the sparseness of sending packets just once and without 'listen-before-talk' may lead to high packet loss in range-critical situations. These unfavorable conditions can be compensated by adapting SF, bandwidth, coding rate and transmission power; however, there is an inevitable tradeoff between these parameters and the transmission time on-air, the possible data output and the energy consumption.

Capacity limitations of LoRaWAN networks due to densification and duty–cycle restrictions are simulated and discussed in [14]. Varsier and Schwoerer [15] found that packet delivery ratios (PDR) reduced to 25% due to packet collisions for a virtual large-scale application with very high node densities. To overcome the limitations of LoRaWAN, more recent studies describe time-slot-based medium access mechanisms. While Piyare *et al.* [16] describe an asynchronous time-division multiple access (TDMA) with a separate wake-up radio channel (range of wake-up radio tested in lab environment, not multi-hop within sub-net), Reynders *et al.* [17] suggest using lightweight scheduling that needs an adoption of the LoRaWAN network.

Particularly relevant for underground (and to some extent also for indoor) applications are factors that affect the quality of radio-based data transmission, like soil layers, asphalt covers, metal structures, interference, and shadowing phenomena. Specifically, Lauridsen et al. [18] calculate a 24 % outage probability for a LoRaWAN communication with an inter-node distance of 2 kilometers and an additional indoor path loss of 30 dB. However, according to the path loss formulas in soil (*cf.* [19]), typical additional path losses for underground locations will be significantly higher than 30 dB, resulting in even higher outage percentages. For example, half a meter of soil already results in a path loss of 40 dB for

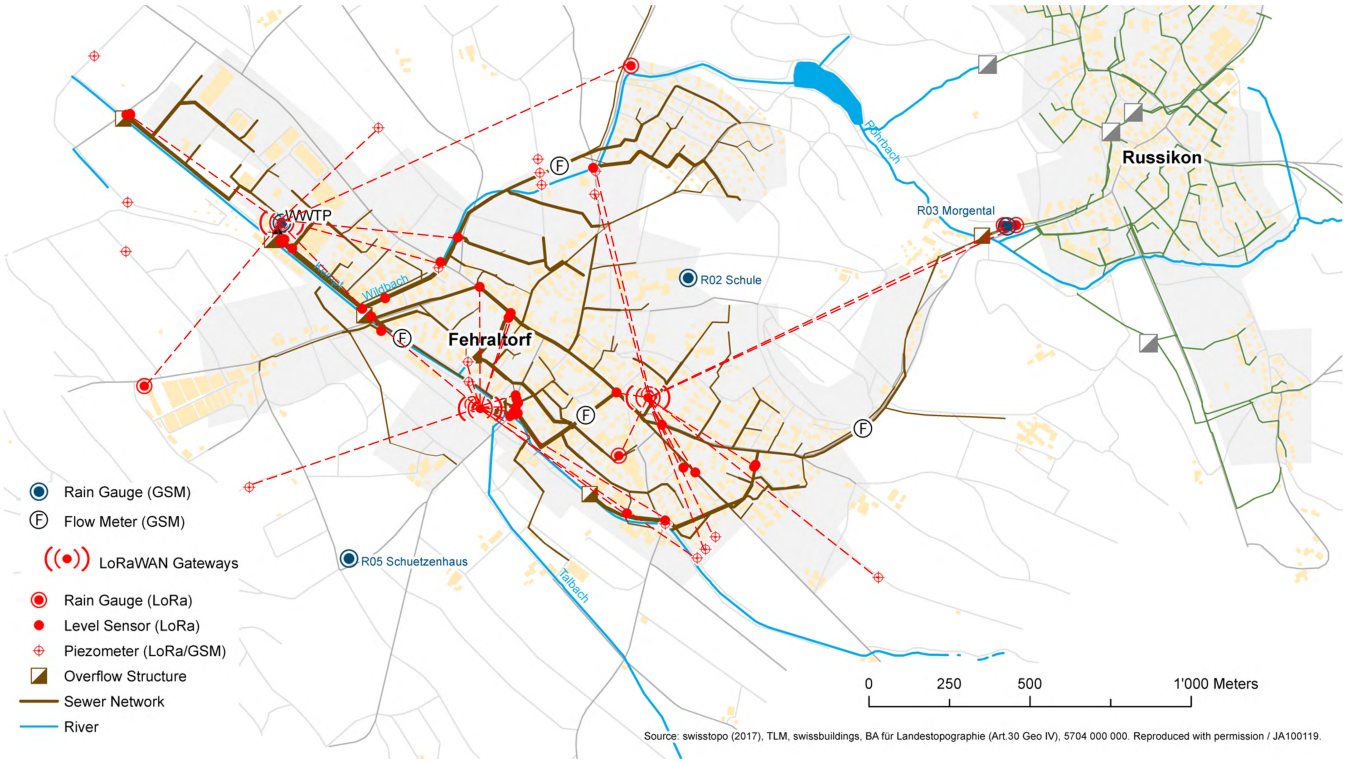

FIGURE 1. **Layout of the wireless sensor network deployed in Fehraltorf (Zurich, Switzerland), using standard LoRaWAN infrastructure. Red markers indicate sensor positions in the sewer network and beyond. Red dashed lines specify radio links from three central gateways to sensor nodes.**

the sub-Gigahertz frequencies used by LoRa. While physical limitations are theoretically known or can be simulated (receiver sensitivity, signal loss, maximum payload, packet collisions [20], [21]), few studies report about the performance of LoRaWANs in real-life environments.

Recently, Lee and Ke [22] proposed a mesh network approach to overcome low packet delivery ratios (PDRs). In the study, which is a temporary proof of concept deployed on a university campus, the authors implemented a LoRa wireless mesh network module based on Semtech's SX1278 transceiver operating in the 430 MHz range. The medium access is controlled exclusively by the gateway, which periodically queries data from each of the joined nodes. Neither of the nodes are allowed to actively send data. This mechanism avoids collisions, but requires that each child node is continuously in 'receive' mode to ensure all query requests are received. Neither power consumption optimization, nor time synchronization were the focus of this study. Another limitation is that the number of supported nodes is limited as each message is forwarded immediately instead of transmitting all received datasets in a single packet to the next node towards the gateway. The proposed concept is based on the fact that (unsynchronized) router nodes must always be awake to forward data from one node to another. This prevents a power down cycle and is not suitable for battery powered devices.

A more recent development is the IEEE 802.11ah (WiFi HaLow) standard [23]. The 802.11ah is a very interesting candidate for underground WSN applications because of its sub-GHz spectrum usage, the open-source character, the option to establish private networks, and the functionality to deploy relays. At the time of this study, however, no WiFi HaLow chipsets were openly available and therefore range and performance benchmarks were not possible.

III. PROBLEM SCOPE AND MOTIVATION

Our research is motivated by the long-term operation of a low-power wireless sensor network deployed in a real-world urban drainage system. With over 60 sensor nodes, 73% of them are installed underground (as of November 2018). The main objective of this initiative is twofold: i) to monitor spatio-temporal dynamics of rainfall-runoff and in-sewer processes in a mid-sized urban settlement over a period of several years (cf. [24]), and ii) to explore the potential and scalability of emerging LPWAN technologies for water resources monitoring in urban areas, which is in the focus of this paper.

To this end, we established a private LoRaWAN as backbone infrastructure for efficient wireless data transmission. Sensors were deployed in early 2016; Fig. 1 illustrates the monitoring layout in November 2018. Today we operate three LoRaWAN gateways that collect data from 62 distributed sensors that monitor rainfall, water levels in rivers and sewers, dielectric conductivity at overflow weirs, air and wastewater temperature as well as groundwater level, temperature and conductivity at a temporal resolution of 1 to 5 minutes.

Whereas various studies discuss performance limitations of LoRaWANs solely based on simulation results [14], [15], [18], our work is based on a quantitative

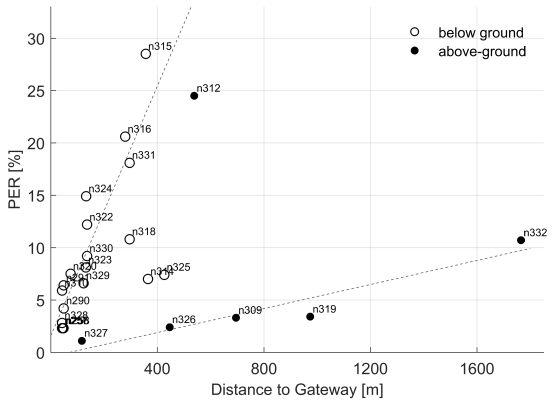

FIGURE 2. Dependence between packet error rate and distance to the corresponding gateway. Observations from 25 sensor nodes over a period of 5 months (Jan 2017–May 2017) were used. Labels represent individual sensor node IDs. Dashed lines indicate linear regression between both subsets (above-/below ground). Node n312 is excluded from the regression analysis due to abnormal failures.

evaluation of long-term field tests in the real-life environment. More specifically, our analysis refers to a 5-month early-stage test period from 01-Jan-2017 to 02-May-2017 with 25 LoRaWAN sensor nodes, 18 of which were positioned below ground. The analyses show (*cf.* Fig. 2):

- a limited reliability of data transmission (12% packet error rate - PER) averaged over 25 sensor nodes,
- an increasing PER with increasing distance to the gateway,
- a significantly different PER increase depending on the radio node position (above / below ground),
- a maximum gateway range of approximately 500m for which reception of packets from below ground nodes is possible.

From this, we conclude that the LoRaWAN technique provides either long-range coverage above ground *or* medium-range underground connectivity, but not both at the same time. Deployment of additional gateways – one possible solution to overcome range limitations for underground applications – was not an option mainly for three reasons: i) gateways usually require AC mains power, ii) costs for gateway installation, management, and internet access increase with the number of installed gateways, and iii) options to place gateways at adequate locations are per se limited (location suitability; permission requirements at private properties).

Another limitation was identified with regard to the time stamping of data packets, i.e. sensor readings. As a time source, sensor networks typically use specialized hardware or a time protocol [25]. In contrast to other techniques, such as NTP on IP-based networks, LoRaWAN does not provide network time distribution to its Class *A* end devices, e.g. through broadcasted beacons. Therefore, uplink data packets cannot be timestamped until they reach the LoRaWAN gateway. According to our analyses, the gateway-timestamps of received sensor values deviate by up to several seconds, depending on the data rate and latency. In case of a more

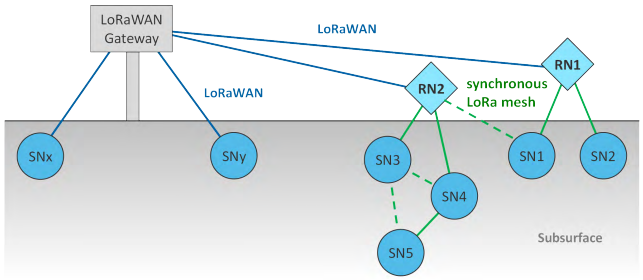

FIGURE 3. Synchronous LoRa mesh topology (RN: Repeater Node; SN: Sensor Node). Dashed lines between synchronous LoRa mesh sensor nodes indicate alternative link paths.

complex 'on-chip aggregation' of sensor readings at the sensor node, this latency further increases. Despite that such an accurate time referencing may not always be of fundamental importance, precise timestamping of sensor readings is relevant when monitoring highly dynamic processes such as rainfall-runoff phenomena in urban drainage. If this deviation becomes too large for the dynamics to be monitored in a given application, more precise time synchronization may be required.

IV. MATERIAL AND METHODS

A. CONCEPT AND SYSTEM ARCHITECTURE

To address previously discussed limitations of the LoRaWAN standard, we propose a novel architecture and concept for medium access control called *synchronous LoRa mesh*. In this section, we discuss the six key aspects of the *synchronous LoRa mesh* concept: 1) conceptualization, 2) physical layer and frame format, 3) network organization, 4) communication cycle, 5) joining process and routing, and 6) the integral time synchronization.

1) CONCEPTUALIZATION

The visible key features are intermediate repeater nodes (RN) that allow for the formation of individual sub-networks, i.e. clusters of sensor nodes (SN) - see Fig. 3. RNs have above-ground LoRaWAN connectivity to a gateway and act as a root for child (sensor) nodes, which are remotely positioned beyond LoRaWAN coverage. To this end, we extend the original LPWAN architecture from a mere star-type towards a hierarchical mesh topology, enabling a multi-hop transmission and thus achieving more flexible routing and extended coverage. Unlike LoRaWAN gateways, RNs operate on batteries and do not need internet access.

Hardware and firmware of RNs and SNs are identical. Both run on the same type of batteries, but nodes fulfill different operational roles. The communication between an RN and corresponding SNs is synchronized with high-precision timing, allowing for coordinated change between sleep mode and wake up within the transmission interval.

2) PHYSICAL LAYER AND FRAME FORMAT

The data exchange between LoRaWAN and the *synchronous LoRa mesh* relies on the same physical layer technology but

TABLE 1. LoRa parameter settings for LoRaWAN (EU863-870) [26] and synchronous LoRa mesh communication.

Parameter		LoRaWAN (EU863-870)	Synchronous LoRa mesh
Spreading Factor	SF	7 – 12 (variable)	9
Bandwidth	BW	125 kHz	125 kHz
Preamble length	nPreambleSymbols	8	8
Transmission Power	P_{Tx}	Variable	+14 dBm
Coding Rate	CR	4/5	4/5
CRC checking		Header & Payload	Header & Payload

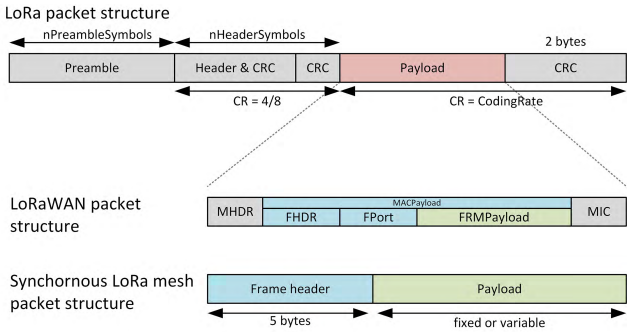

FIGURE 4. Relation between the standard LoRa packet structure (Explicit Header Mode) [31] and the synchronous LoRa mesh packet frame that is inserted in the payload section.

slightly different transmission parameters are used (Table 1). For the sake of simplicity, the *synchronous LoRa mesh* uses a fixed spreading factor and a fixed transmission power. Both can be configured before deploying the RNs and SNs.

In contrast to this simple approach, devices in the LoRaWAN network can inform the network server whether it should control their transmission power and spreading factor or not. In case this feature is enabled, the network server will try to lower a device's spreading factor when the quality of the received signal is sufficient. This mechanism is called adaptive data rate (ADR) control [26].

The LoRaWAN as well as the synchronous LoRa mesh packets both use the LoRa packet format defined by Semtech [11]. However, they differ regarding the organization of the available payload (see Fig. 4). LoRaWAN includes a one-byte MAC Header (MHDR) field at first position containing information about the message type and used protocol version. The Frame Header field (FHDR) contains the address of the receiving device, and other control and acknowledgement information, whereas the port field (FPort) defines which of the 223 available ports is used for packet delivery. The actual application payload is included in the MAC Frame Payload Encryption (FRMPayload) field. Data integrity in LoRaWAN is checked by a message integrity check using the MIC field.

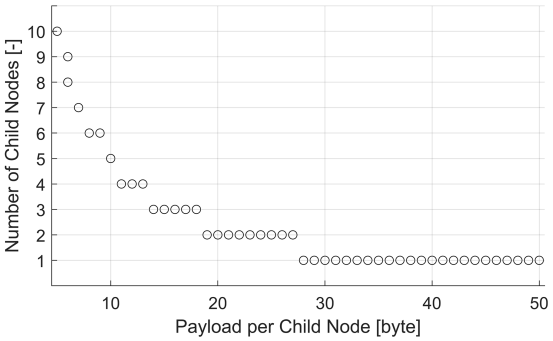

FIGURE 5. Number of child nodes within a sub-network corresponding to the possible payload size. This estimation assumes worst-case transmission parameters for the repeater node, i.e., SF12 (DR0) with a maximum total payload of 51 bytes.

In contrast, the *synchronous LoRa mesh* payload format is simpler. A five-byte Frame header contains information about destination, source address, and the type of the current packet (e.g. data or synchronization). Depending on this packet type, the payload contains a variable or fixed amount of data bytes. In case of a packet of the type *data*, the length information is delivered within the payload field.

3) NETWORK ORGANZATION

Communication within the *synchronous LoRa mesh* sub-network is based on the *synchronous LoRa mesh* protocol allowing SNs to transmit their own data, but also to forward data packets from other SNs. More specifically, the routing algorithm enforces packet forwarding along a dynamically established tree-type structure with the RN as root node. This applies for the data flow in both directions, from the terminal SN upwards through other SNs and the RN to the gateway (uplink) and reverse from the gateway through the RN and other SNs to the terminal SN (downlink).

LoRaWAN communication can dynamically operate at the lowest possible data rate (DR0) [25], [26]. In the worst case, the packet payload is limited to 51 bytes. A RN compresses data received from all connected SNs into a single LoRaWAN packet, thus the number of supportable SNs per RN must not exceed the maximum possible payload of LoRaWAN. Fig. 5 illustrates the interdependence between the number of child nodes in a sub-network and payload.

4) COMMUNICATION CYCLE

Fig. 6 exemplifies the sequence of individual slots during a *synchronous LoRa mesh* communication cycle. The RN assigns individual up- and downlink slots for each joining node in the sub-network. Contrary to LoRaWAN, medium access in *synchronous LoRa mesh* sub-networks is based on a TDMA mechanism. In typical TDMA systems, each member is assigned a time slot for the transmission of data. However, *synchronous LoRa mesh* differs from this approach by allocating *receive* instead of *transmit* slots. In the traditional approach, nodes have to wake-up and switch to receive mode every time when one of its neighbors reaches the assigned

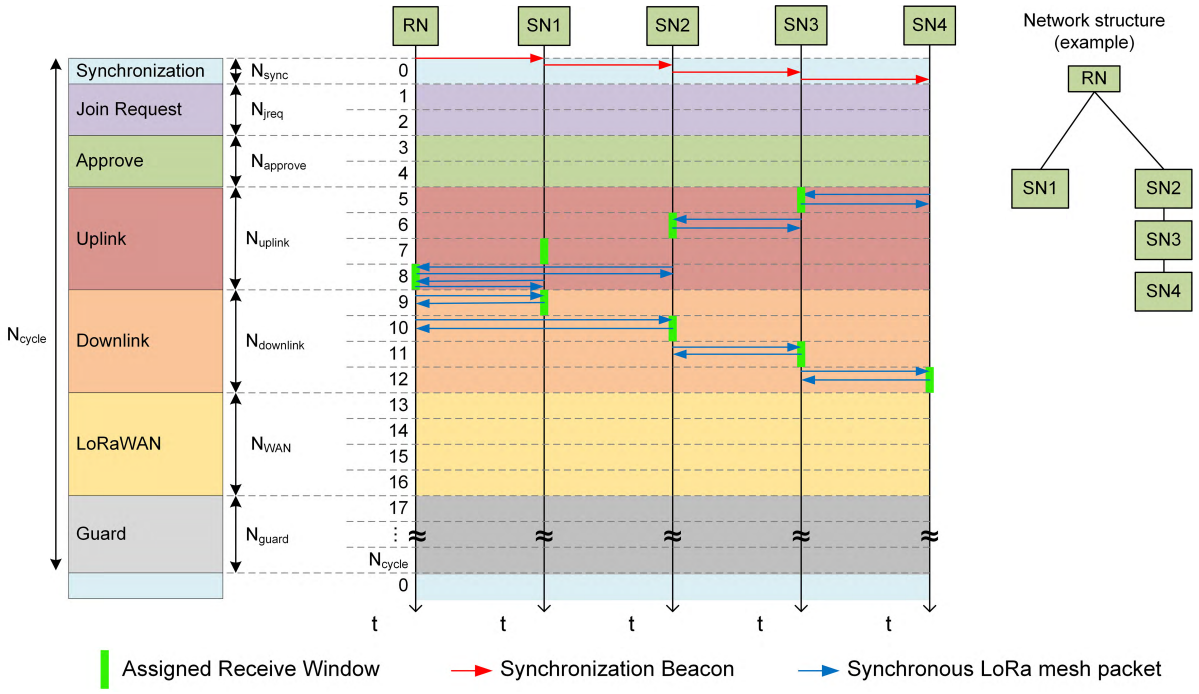

FIGURE 6. Timeslot allocation in a synchronous LoRa mesh cycle for a given example sub-network (right). Center: Detailed message exchange during synchronization, up- and downlink phases. The scheme shown here represents a specific example for a sub-network structure containing four child nodes. The ∼ sign in the guard slot indicates that the period/window for this slot is longer than the other slots, acting as a buffer.

transmit slot. The *synchronous LoRa mesh* approach reduces energy consumption as nodes have to wake-up only once and be in receive mode during their specific receive time slot.

The responsible parental RN administrates a discrete-time communication cycle that is sub-divided into fixed time slots. Organizing communication in time-slots avoids packet collisions and reduces times in energy-demanding receive mode. As a result, the overall power consumption is minimized.

In the communication cycle for a given example of four child nodes and two branches (*cf.* Fig. 6) the first time slot #0 is assigned to the synchronization phase of the sub-network. The following time slots #1 to #4 are reserved for the join and approve process. The central slots #5 to #12 are allocated to the transmission of payload data, either for up- or downlink communication. In this example, timeslot #7 remains unused as no child node is connected to SN1, thus SN1 has no data to receive. Time slots in the LoRaWAN phase #13 to #16 are exclusively used by RNs for the LoRaWAN communication with the gateway. A cycle is completed by so-called guard slots #17 to N_{cycle}. During these slots, all nodes in a sub-network are inactive. This ensures adherence to the required LoRaWAN duty cycle restrictions, commonly set to 1% (*cf.* ETSI EN300.220-V1, V2.4.1 standard, [26]) and enables the parallel operation of other sub-nets.

To minimize latency, the latest time slots in the uplink time slot group are assigned first, i.e. the child nodes located closer to the RN will get their receive windows later than those located farther away. This approach increases the probability that packets are forwarded to the RN within a single cycle. The assignment of time slots is reversed for downlink communication.

In contrast to the LoRaWAN standard, each SN in the sub-network always acknowledges the reception of a packet. In case a transmitted packet is not acknowledged, data can be stored on the local SD card. This avoids data loss, as packet repetition is not possible due to the limited LoRa payload.

The cycle illustrated in Fig.6 exemplifies a sub-network with four SN. As described, the number of sub-slots is configurable and dependent on the minimum number of SNs required within the sub-net, the selected data rate and payload within the sub-net, the duty cycle restrictions, and the minimum total cycle time.

5) JOINING PROCESS AND ROUTING

RNs operate as root nodes of a sub-network, SNs proceed with a join process to participate in the network. There are two ways that unattached SNs can join a sub-network: in a *direct join,* where an SN communicates directly with an RN; or an*indirect join,* where an SN is not able to reach an RN directly and the SN has to join via another already connected SN. In both cases, a newly powered SN first scans the channel for existing sub-networks. The integration of an unattached SN to a particular sub-network is based on periodically transmitted beacons. Beacons are 7 byte long data packets containing a current timestamp and 3 byte control data. According to the signal strength of these beacons, the joining SN selects either an RN or an SN as a join agent.

For a direct join, the SN sends a join request to the RN which is immediately answered with the assigned time-slot. In the case of an indirect join, the concept is to propagate the join request of the remote SN upwards to the RN and send down a so-called new node packet so that all sensors on the route can update their routing table. This completes the integration of the SN into the sub-network.

From this point, each SN is capable of calculating the required wake-up times according to the cycle-settings and the assigned time slots. These wake-up times define the RTC alarms, which cause each SN to exit the low power state.

A newly activated RN must consider other RNs with their sub-networks. To prevent the added RN from interfering with the communication of another sub-net, the RN first scans the channel and listens for beacon packets. After this search, it chooses the start time of its own cycle in the middle of the largest unused time range.

6) TIME SYNCHRONIZATION

High-precision time synchronization is essential for an energy-efficient and conflict-free communication of RN and SN in a sub-network. Additionally, it allows an absolute timestamping of measured sensor values directly at the origin. Synchronization of all SNs in a sub-network is ensured through beacons that are forwarded over several hops using a *beacon flooding* approach (see Fig. 7). Details of the beacon forwarding are illustrated in Fig. 8. The RN initiates the synchronization at the beginning of each cycle transmitting a beacon packet containing the current system time (t_{sys0}). Each SN repeats the beacon within an assigned forwarding window (assignment during join). The beacon packet reaches the SNs with a latency caused by the processing time (t_{proc}) of the microcontroller and the time on air of a beacon packet (TOA_{beacon}). The latter causes the majority of the delay and can be calculated according to the transceivers datasheet [31]. The processing time of the microcontroller includes interrupt latencies, time for data processing, and serial communication, etc. It was measured during development. Thereby, each SN is able to calculate the actual system time (t_{sys1}) by taking into account the used forwarding window (i_{FW}), the forwarding window duration (T_{FW}), the processing time (T_{proc}) and the time on air of the beacon packet (TOA_{beacon}), see (1). This periodical re-synchronization prevents the network from exceeding time drifts.

$$t_{sys1} = t_{sys0} + i_{FW} * T_{FW} + T_{proc} + TOA_{beacon} \qquad (1)$$

The system time transmitted by the RN (t_{sys0}) corresponds to the coordinated universal time (UTC). Thus each joined node is provided with UTC information that allows independent but absolute timestamping of the captured measurement values. Consequently, the relative time accuracy among the nodes of a sub-network is independent of the chosen time source. Only the RNs need to retrieve the actual UTC time using an external time source.

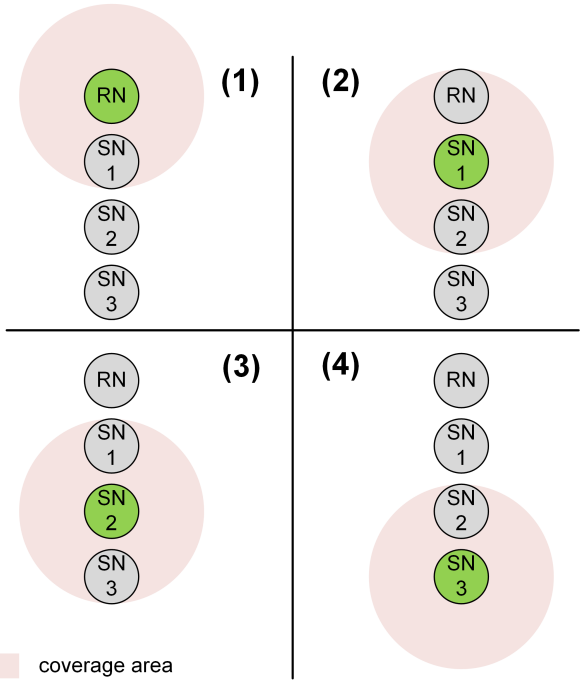

FIGURE 7. Illustration of the synchronization process. The beacon is propagated through the whole sub-network starting from the repeater node (RN). Each node forwards the beacon to supply neighboring nodes with time information.

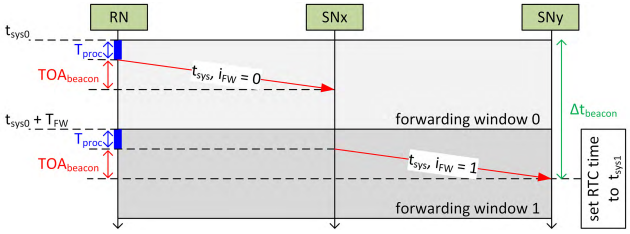

FIGURE 8. Detailed beacon forwarding process using TDMA to avoid collisions. Each node repeats the beacon within a defined forwarding window. The receiving node is then able to compensate time offsets caused by the time on air of the radio packet (TOA_{beacon}).

As RNs are typically located above-ground, it is assumed that they have access to at least one external time source to synchronize their internal real-time clock (RTC) to the UTC.

For the proposed system, we implemented and tested two options for central time retrieval, also to illustrate flexibility:

- In Central Europe, the time signal transmitter DCF77 located in Mainflingen, Germany provides a long ranging (2000 km) time signal at 77.5 kHz [27]. Although the use of DCF77 is geographically restricted to Europe, the concept itself can also be applied to other regions where a time signal transmitter is available, such as WWVB in the U.S. or BPC in China.
- Alternatively, inexpensive GPS receiver modules can be used. To reduce energy consumption of such GPS modules (they draw up to 30mA), their on-air time may be minimized to short periods and only when the internal RTC has to be re-adjusted.

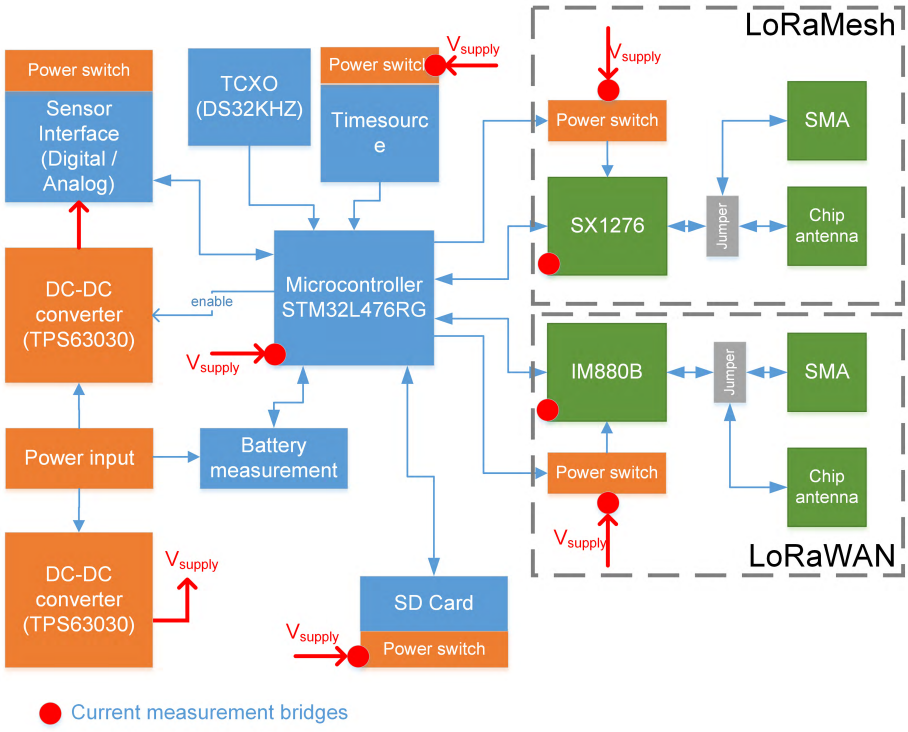

FIGURE 9. Block diagram (orange: a) power supply system, blue: b) microcontroller and peripherals, green: c) radio part).

The required update frequency of the calendar time in the RN depends on the desired precision of the time-stamps. Following the low-power concept, it may be sufficient if the internal real-time clock is set initially at the power-up and, later on periodically, e.g., once a week, aligned with the reference time.

B. HARDWARE AND FIRMWARE

The design consists of four main parts: 1) power supply system 2) microcontroller and peripherals, including sensor interfaces, 3) radio part, and 4) firmware. 9 shows the block diagram including specifications of the hardware used for the prototype node. The identical hardware is applied for RNs and SNs.

1) POWER SUPPLY AND ENERGY MANAGEMENT

Two DC-DC converters provide two separated power supply paths. While one of the converters supplies the sensor interface, the other converter powers the microcontroller and all other components. The design allows a high flexibility for power-down modes. In addition, it provides the infrastructure for individual power measurements of each component. Moreover, each of the peripherals can be separated from the power supply using power switches (see Fig. 9), preventing them to consume energy when they are not in use.

Minimization of energy consumption was one of the key requirements, mainly to allow long-term operation with least possible maintenance. The design goal was to enable a self-contained network operation of at least one year on two C alkaline cells in series, assuming a 5 minute transmission interval. This corresponds to a capacity of approximately 6000 mAh and a maximum energy consumption of 29 μ Ah per cycle. RNs and SNs must be power efficient in order to comply with this requirement. Our measurements confirm that the most power-intense part is the LoRa communication phase. Consequently, this phase – representing a compromise between payload, range conditions and time-on-air – must be kept as short as possible. To address this aspect, *synchronous LoRa mesh* nodes enter a low-power mode when no data transmission or measurement is ongoing (see Fig. 12). The real-time operating system (RTOS) of the microcontroller automatically powers down during RTOS's IDLE state. The system wake-up is interrupt-driven and triggered via real-time clock.

2) MICROCONTROLLER AND PERIPHERALS

Heart of the control section is an ST Microelectronics STM32L476RG CPU with an ARM Cortex-M4 core optimized for low-power applications. A temperature-compensated crystal oscillator (TCXO) provides a precise 32.768 kHz digital clock signal with an accuracy of $\pm$7.5 ppm.

The reference time signal is provided either through DCF77 or GPS. An interface for the connection of these external time source systems is included. The interface provides a switchable power supply (GND and VCC), as well as TX and RX line connected to an UART-interface of the MCU.

We provide proof of concept for both external time sources, DCF77 and GPS. The FUM DCF V1 [28] was chosen to retrieve the current time via the DCF77 system. The FUM DCF V1 module receives and decodes the signal from the DCF77 transmitter and delivers a digital time signal to the MCU at the start-up and further regular intervals. It consumes a typical current of 20 μ A in standby mode and 1.6 mA when receiving the time signal. The Ultimate GPS Breakout from Adafruit [29] determines the current time by using the GPS system. After the module powers on, it starts with the localization process. The current world time is provided after localization is complete.

The sensor interface is designed to be compatible with a wide range of sensors and interfaces (SPI, UART, OneWire and I2C). Additionally drivers for RS-485, RS-422 and RS-232 protocols are placed on the design. At least two analog inputs are reserved for the sensor interface, which allows for the connection of sensors with analog signal outputs.

To avoid losing valuable sensor data in case of an unexpected failure or a weak network connection, nodes include a micro SD card interface to store measured sensor data locally. Data that are lost during wireless transmission can be restored by retrieving data manually from the micro SD card. The micro SD card capacity is 8 GB that allows storing measurements (typically 26 bytes) in 5 minute resolution for several years. To further reduce power consumption, the micro SD card option can be disabled or completely left out in a hardware re-design.

The microcontroller can supervise the battery voltage. A high side switch connects the battery voltage over a voltage divider with one of the available analog-to-digital converter inputs of the microcontroller.

3) RADIO FREQUENCY (RF) PART

The communication in the *synchronous LoRa mesh* sub-network has the same physical data transmission technology as LoRaWAN. For the LoRaWAN and the *synchronous LoRa mesh* part of the system, actually two separate transceivers are used even though a single transceiver (e.g. an SX1276 radio chip, Semtech Corporation) could handle both communications, the LoRaWAN as well as the *synchronous LoRa mesh*.. Using the two separate transceivers was a practical decision rather than a technical need. For the proof of concept, we used a compliant and tested LoRaWAN stack implementation on a module and focus development work on the *synchronous LoRa mesh* protocol implementation.

The LoRaWAN communication is realized with the iM880B module (IMST GmbH) - a fully integrated LoRaWAN compatible transceiver module [30]. It includes the SX1272 transceiver from Semtech [31] and a STM32L151CxU6A MCU from ST (STMicroelectronics, 2017). IMST provides a complete LoRaWAN firmware including a host controller interface (HCI). The iM880B module also provides different digital interfaces (UART, SPI and I2C). The module can be fully controlled through the UART interface [32]. The module transmits data received from the UART interface to a LoRaWAN gateway. Data from the gateway is digitally available after reception.

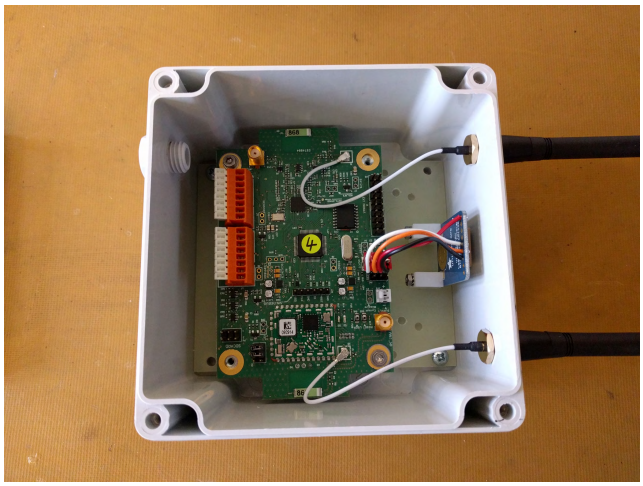

FIGURE 10. Hardware configured in a repeater node (RN) prototype.

FIGURE 11. Hardware configured in a sensor node (SN) prototype.

Although the basic PCB hardware is identical, two assembly configurations were used for the field tests: a) RN configuration (Fig. 10) and b) SN configuration (Fig. 11). The RN configuration includes the external time source (DCF77 or GPS module) and an additional antenna for the LoRaWAN up-link.

4) FIRMWARE CONCEPT

The firmware is based on the FreeRTOS [33] real time operating system, which controls the timing of several processes. Currently, two different tasks are implemented. A run task handles operation during the active phase of the cycle, whereas the idle task is activated during the inactive phases of the cycle. The latter controls the MCU's low-power features.

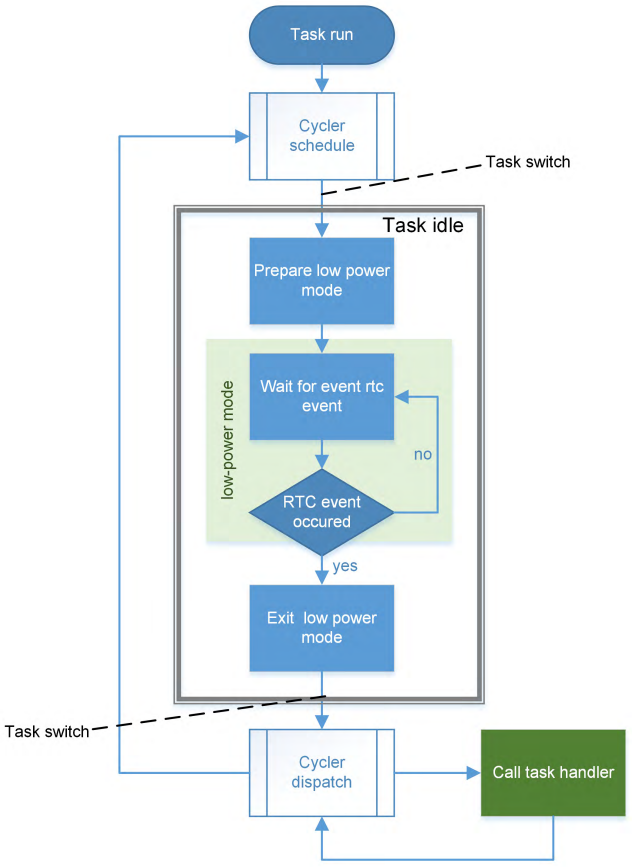

FIGURE 12. Firmware concept including low-power modes.

The firmware concept is illustrated in Fig. 12. After power-up, software execution starts with the run task (*Task run*). The central module is the cycler, which controls the software sequence by calling other modules at a given time and in the right order. After scheduling all registered jobs, (*Cycler schedule*) the system switches to the idle task (*Task idle*). This task is responsible for the initiation of the low-power mode (*Prepare low power mode*) by disabling peripherals to avoid unnecessary power consumption. After preparation, the MCU's low-power mode is activated and the controller remains in an energy saving state until the RTC reaches a previously calculated alarm time (see Section IV, A, 6). As the cycle's settings are configured on each RN and SN, the nodes are capable of calculating this alarm time independently. An RTC alarm in turn triggers an interrupt which causes the system to immediately switch back to active mode by re-enabling all peripherals and setting the microcontroller back to an active state. The RTOS again performs a task switch to reactivate the run task. Now the cycler module is able to start up a given job (e.g. Downlink-Communication). By using the RTC module of the microcontroller as timing reference, all other components can be disconnected from power supply and the controller can be switched to low power state "Stop 2 Mode". This mode of operation is the most energy saving, while the controller does not have to reboot after exiting [34].

V. FUNCTIONAL AND PERFORMANCE TESTS

In order to ensure adequate functionality and evaluate the system performance, we carried out systematic tests in the laboratory and in the field.

A. FUNCTIONAL TEST

In a first step, we performed *laboratory* experiments with 12 sensor nodes and 6 repeater nodes to check the functionality of hardware and firmware.

1) NETWORK SETUP

The most important test was a stress test, where we set up all the nodes next to each other and then switched them all on at the same time. In this scenario, all nodes are within the mutual reception range. All nodes must first wait until all sub-networks have been established, send out the repeater beacon signal, and then attempt to join to a repeater successfully.

2) ENERGY CONSUMPTION

The power consumption within a sub-network was measured for one RN and one SN under real-life conditions for a cycle duration of 5 minutes. For the tests DS18B20, temperature sensors were connected to the SN. The cycle includes the measurement, the storage of the measurement value on an SD card, and the radio transmission. Power consumption was measured using a Keysight's DC Power Analyzer N6705C with an N6781A 2-quadrant source/measurement unit.

The energy consumption of a single SN for one communication cycle is 370 mJ with a supply voltage of 3.2 V. The RN consumes 670 mJ when *two* SN are integrated in the sub-network forming a simple tree; the LoRaWAN transmission is realized with a spreading factor of 9 (SF9).

Still, the energy consumption within a sub-network *varies* depending on i) the position of the participating SN in the hierarchy, and ii) the topology type of the sub-network. Generally, the higher up in the hierarchy, the more power an SN consumes since it receives and acknowledges data from one or more nodes at deeper levels. In case of a *line topology* in a sub-network, i.e., SNs are aligned in series, the amount of data forwarded to the next hierarchy level accumulates the further the communication moves towards the RN (data sink). For an example configuration (SF9, 10 bytes payload per node), the consumed energy *increases* by 12 mJ per hierarchy level (adding to the total consumption of one SN of 370 mJ). In case of a *branched sub-network*, the energy consumption of child nodes at higher level is determined by the number of receive/send windows and downlink transmits (ACK's). For the same example configuration (SF9, 10 bytes payload), but as a branched tree, the energy consumption increases by 43 mJ per branch. It is clear that communicating in a line topology sub-network is less energy intensive.

Overall, we observe that RNs consume about twice as much energy as SNs, mainly because of the additional LoRaWAN communication with the gateway. Still, both

TABLE 2. Statistics of synchronization accuracy (15 measurements).

Measurement	Offset
Minimum offset	63.28 µs
Maximum offset	551.6 µs
Mean offset	253.35 µs
Standard deviation	132.04 µs

device types, RNs and SNs, operate on the same type of batteries. AC mains power is *not* required to power RNs. To minimize maintenance effort, RNs can optionally be equipped with energy harvesting modules, such as solar cells, since RNs are typically located above ground.

3) SYNCHRONIZATION ACCURACY

The synchronization accuracy describes the time offset between the repeater and the sensor node. To measure this offset, a GPIO pin on SN and RN is set at the beginning of a communication cycle and both signals are connected to an oscilloscope. The offsets listed in Table 2 result from 15 measurements for the tested implementation.

B. FIELD TESTS

We conducted two independent long-term field tests under real-world conditions to analyze the *synchronous LoRa mesh* sub-network performance. The tests included the functionality regarding alternating connectivity between distinct SNs and different RN, potential conflicts during packet transmission according the time-slotted protocol, and the integration of the *synchronous LoRa mesh* sub-network into the overall LoRaWAN network, including the packet delivery performance.

1) PERFORMANCE INDICATORS

For both field tests, we recorded operating parameters from the LoRaWAN network. For this purpose, we have placed standard LoRaWAN nodes as reference nodes next to *synchronous LoRa mesh* SNs. Parameters such as SNR, RSSI and SF from reference nodes and *synchronous LoRa network* RNs were recorded. We analyzed their evolution over time and their interdependence. We evaluated the reliability of data packet delivery for each individual node using the packet error rate (PER), i.e. the ratio between the number of at the gateway received packets (# RECEIVED) and the number of packets that should have been received (# EXPECTED) within a given evaluation period, T:

$$\mathrm{PER_i} = 1 - \frac{\sum_T \#\mathrm{RECEIVED_i}}{\sum_T \#\mathrm{EXPECTED_i}} \tag{2}$$

The estimation of the number of expected packets assumes a device-specific, but constant transmission interval. For the *synchronous LoRa mesh* being a multi-hop system, counting the number of packets arriving at the gateway (GW) accounts for both the packet loss during the *synchronous LoRa mesh* communication (SN-RN), and the LoRaWAN based communication (RN-GW). In our evaluation however we do not differentiate the link where the packets are lost; instead, we quantify an overall system performance for each individual *synchronous LoRa mesh* sensor node.

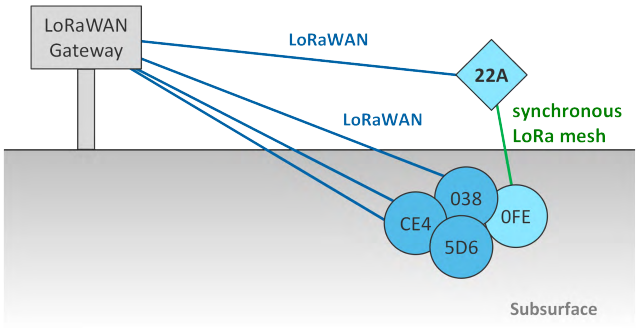

FIGURE 13. Experimental layout of the first field test in a service shaft of a district heating system.

FIGURE 14. Synchronous LoRa mesh and LoRaWAN reference nodes in the service shaft in 3 m depth were mounted next to each other.

2) FIELD TEST 1

The first field test was carried out in a dense urban area in the city center of Basel, Switzerland (300,000 inhabitants). For a period of 23 days, we compared one *synchronous LoRa mesh* system (repeater and sensor node) with three different off-the-shelf LoRaWAN sensor nodes (2x DecentLab, RisingHF) - see Fig. 13. Both LPWAN systems essentially connected to one and the same gateway in 2000 m distance. The sensor nodes were installed next to each other, three meters below ground, in a service shaft of a district heating system (see Fig. 14, 15).

The *synchronous LoRa mesh* repeater was positioned above-ground at a lamppost at a height of 4 m and 23 m away from the service manhole. The transmission interval was set to 2 minutes for the *synchronous LoRa mesh* SN and to 1 and 10 minutes, respectively, for the LoRaWAN reference nodes.

Fig. 16 illustrates the relative packet loss during a 3-day period at which all participating nodes were forced to

FIGURE 15. Closed service shaft cover made of steel and concrete.

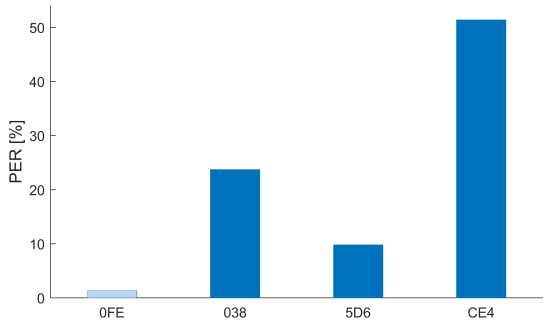

FIGURE 16. PER observed in the test period of 25 28/05/2018 of the synchronous LoRa mesh sensor node (0FE) and the reference nodes (038, 5D6, CE4). Note the different transmission intervals ofindividual nodes (0FE – 2 min; 038 - 1 min; 5D6 – 10 min; CE4 – 1 min).

FIGURE 17. Repeater node (RN) position at a lamppost.

transmit on the same SF level. While the packet loss of the *synchronous LoRa mesh* system (node ID: 0FE) remains very low (1.3 %), losses for reference nodes range from 9.7 % up to 51 %, depending on the reference node manufacturer and the transmission interval. Note that the PER recorded for the *synchronous LoRa mesh* system includes the packet loss for both 'hops'- the one from sensor node to the repeater node and the one from repeater node to the gateway. These results underline the superior performance of the *synchronous LoRa mesh* system with regard to the reliability of packet delivery.

Extended analyses for the full 23 day test period confirm the results from the selected 3-day evaluation period. Despite that the reference nodes transmitted with varying SF levels (with ADR option enabled), the PER still remained higher compared to the *synchronous LoRa mesh* system. It can be concluded that a more favorable SF level (less transmission time, reduced risk of packet collisions) does not significantly influence the transmission performance.

3) FIELD TEST 2

The second field test was carried out in the center of the municipality of Fehraltorf located 12 km northeast of Zürich, Switzerland (moderately dense urban area, primarily two-story housing, 6400 inhabitants). In this test, a total of 16 *synchronous LoRa mesh* nodes were deployed for a total period of 45 days (March – April 2018): 11 SNs at underground sewer manholes (Fig. 19), and 5 RNs above-ground at nearby lampposts at 3 m height. *Synchronous LoRa mesh* hardware was deployed in three distinct clusters (see Fig. 18). All RNs (one is shown in Fig. 17) connect to one and the same LoRaWAN gateway (Wirnet Station 868, Kerlink). The distances between the gateway and individual repeater are 170 m, 370 m, 630m, 750 m and 1830 m respectively.

At five of the 11 SN locations, a LoRaWAN reference SN (manufacturer: Decentlab-GmbH, Switzerland, 2018) was installed in parallel. The transmission interval of all SNs was set to 5 minutes. The data packet of a single SN has a size of 8 bytes and thus packets of up to five SNs plus the repeater state can be forwarded by a RN through the LoRaWAN network in a single transmission (maximum payload size is 51 bytes at DR0 / SF12). The data rate within the *synchronous LoRa mesh* sub-network was set to DR3 / SF9 to allow sufficient range from the underground and to keep the sub-slot duration short.

Fig. 20 compares the relative packet loss (PER in %) for 11 sync*hronous LoRa mesh* sensor nodes (light blue) and 5 LoRaWAN reference sensor nodes (dark blue). Over an evaluation period of 45 days, we observe a very low packet loss of 2.2 %, averaged over all *synchronous LoRa mesh* systems deployed in this test.

LoRaWAN reference nodes on the other hand showed a significantly higher packet loss – at three out of five locations at which reference nodes were installed, no connection to the gateway could be established throughout the entire period.

Note that both, the packet loss via the LoRaWAN transmission (above-ground) and the loss via the transmission within the sub-network, contribute to the total PER. The PER contributions vary moderately; the loss within the *synchronous LoRa mesh* sub-network remains lower than 2%.

Interestingly, while signal routing for most *synchronous LoRa mesh* systems remained unchanged, one of the

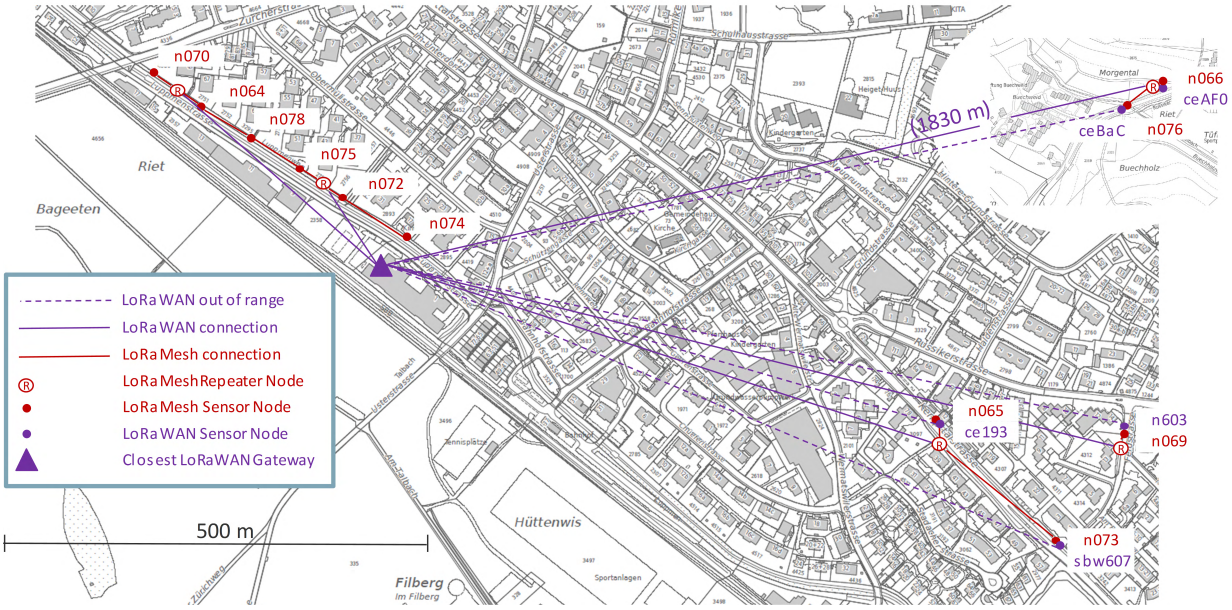

FIGURE 18. Experimental layout of field test 2. Three distinct synchronous LoRa mesh clusters were established.

FIGURE 19. Uninviting conditions: Synchronous LoRa mesh sensor node mounted at a manhole ladder in a sewer shaft (temporary installation).

synchronous LoRa mesh sensor nodes (n073) interchangeably connected to two different repeater nodes. This phenomenon confirms a flexible signal routing, which effectively makes *synchronous LoRa mesh* systems more resilient against unforeseen range limitations.

VI. LIMITATIONS AND FUTURE WORK

The maximum number of child nodes in a *synchronous LoRa mesh* sub-network is *per se* limited to five SNs due to the inherent payload restriction of the LoRaWAN standard. Assuming worst case conditions for the LoRaWAN link between RN and gateway, a payload of 51 bytes per cycle must not be exceeded. Depending on the given data rate setting, and depending on how much data is required to be transmitted, the number of child nodes can however vary. Fig. 5 in Section IV, A, 3 illustrates various sub-network configurations assuming worst-case data rate settings (DR0).

Future work will focus on analyzing the dependencies of individual sub-networks with different configurations of cycle time, number of sub-slots, data rate, and channel allocation.

More research is required to prevent single-point failure mechanisms. Worst-case scenario testing in the field showed the need for a fail-safe mechanism. This is useful to prevent the battery from getting depleted rapidly in case an SN keeps unsuccessfully attempting to join a sub-network. This scenario can occur, for instance, when the corresponding RN is out of operation and no other RN is within the SN's reception range.

The *synchronous LoRa mesh* concept enables sub-network routing over multiple hops. One of the future tasks is to fully stress-test this multi-hop functionality. So far, only the single-hop implementation has been extensively field-tested.

In this phase of the work, security aspects have not been addressed. While LoRaWAN itself employs an AES 128 encryption, no security mechanisms have yet been implemented for the *synchronous LoRa mesh* sub-network. Introducing a security concept will reduce the available payload size and therefore may further limit the number of supportable nodes in a sub-network.

Current hardware design separates radio transceivers for the *synchronous LoRa mesh* and the LoRaWAN part. This is not strictly necessary because only one mode is active at a time. By adding the LoRaWAN stack to the MCU only one radio transceiver is needed, which decreases the hardware costs and size. However, the independent implementation of the LPWAN part and the *synchronous LoRa mesh* allows for

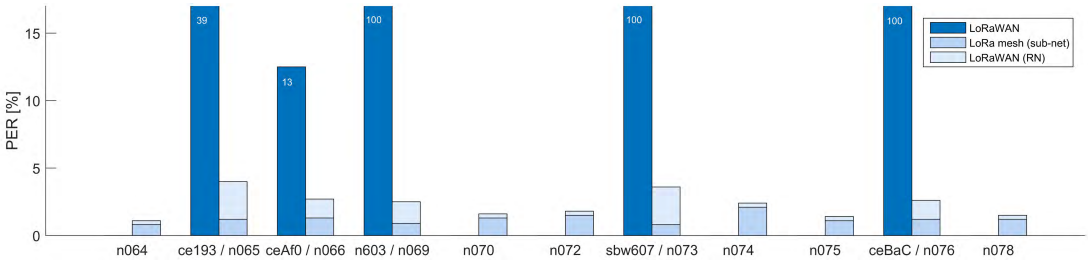

FIGURE 20. Total PER for selected underground monitoring locations (node IDs at x-axis; see spatial reference of nodes in Fig. 18) to compare i) the standard LoRaWAN network (dark blue bars) and ii) *the synchronous LoRa mesh* network (light blue bars). A PER of 100 % indicates that there was no radio coverage before introducing the extended routing.

an exchange of the WAN communication technologies (e.g. LTE NB-IoT) while the sub-network remains unchanged.

Despite the significant improvements regarding the quality of service, our results show that the packet loss occurring in the LoRaWAN part dominates the overall WAN performance (*cf.* Fig. 20). Still, this limitation cannot be attributed to the *synchronous LoRa mesh,* but it needs to be taken into account.

VII. CONCLUSION

Despite the rapid evolvement of promising Low-Power Wide Area Network systems, transferring process monitoring data from remote or underground facilities with high signal path attenuation, such as urban drainage systems, remains a major challenge in terms of range, packet loss rate and energy consumption.

This paper has discussed this problem by means of a systematic evaluation of an ongoing multi-year field experiment. The authors have addressed existing limitations with the development of a meshed and LoRa modulation-based concept that allows underground sensor nodes to integrate into existing LoRaWAN networks using intermediate repeater nodes. The developed hardware of both node types is similar; all nodes operate on standard batteries in ultra-low-power mode. Key aspect is a time-slot-based transmission between precisely synchronized sensor and repeater nodes. Beyond mere implementation, the concept has been successfully tested and thoroughly evaluated in two full-scale field trials with a total of 17 prototype devices.

With the *synchronous LoRa mesh* the authors have shown that formerly difficult to integrate sensors located underground can be connected to an existing LoRaWAN.

Full-scale field trials show that with the *synchronous LoRa mesh* approach the transmission quality significantly improves, and thus packet error rates drop, despite a high signal attenuation. Therefore, the system makes a valuable contribution to enabling data-driven research of high resolution spatio-temporal dynamics. In urban water infrastructure management, this technology is expected to ease the collection of distributed information, while increasing the quality and consistency of data sets.

ACKNOWLEDGMENT

The authors would like to thank Simon Dicht, Benjamin Häring, Fabian Frei, and Philipp Bachmann. Without their great efforts in the field tests and the completion of the hardware and software, we would not have been able to realize the project. Special thanks go to Dominik Baumgartner from the municipal utilities of the city of Basel (IWB) and the municipal administration of Fehraltorf. We furthermore acknowledge the valuable feedback of three anonymous reviewers, and we thank Eawag for the financial support of this research.

REFERENCES

[1] B. Kerkez *et al.*, "Smarter stormwater systems," *Environ. Sci. Technol.*, vol. 50, no. 14, pp. 7267–7273, 2016.

[2] S. Eggimann *et al.*, "The potential of knowing more: A review of data-driven urban water management," *Environ. Sci. Technol.*, vol. 51, no. 5, pp. 2538–2553, 2017.

[3] U. K. Maheepala, A. K. Takyi, and B. J. C. Perera, "Hydrological data monitoring for urban stormwater drainage systems," *J. Hydrol.*, vol. 245, nos. 1–4, pp. 32–47, 2001.

[4] U. Raza, P. Kulkarni, and M. Sooriyabandara, "Low power wide area networks: An overview," *IEEE Commun. Surveys Tuts.*, vol. 19, no. 2, pp. 855–873, 2nd Quart., 2017.

[5] A. R. da Silva, M. Moghaddam, and M. Liu, "The future of wireless underground sensing networks considering physical layer aspects," in *The Art of Wireless Sensor Networks* (Advanced Topics and Applications), vol. 2, H. M. Ammari, Ed. Berlin, Germany: Springer, 2014, pp. 451–484.

[6] H. T. H. Trang, L. T. Dung, and S. O. Hwang, "Connectivity analysis of underground sensors in wireless underground sensor networks," *Ad Hoc Netw.*, vol. 71, pp. 104–116, Mar. 2018.

[7] J. Bardyn, T. Melly, O. Seller, and N. Sornin, "IoT: The era of LPWAN is starting now," in *Proc. ESSCIRC Conf. 42nd Eur. Solid-State Circuits Conf.*, 2016, pp. 25–30.

[8] LoRa Alliance. (2015). *LoRaWAN What is it?—A Technical Overview of LoRa and LoRaWAN LoRa Alliance*. [Online]. Available: https://www.lora-alliance.org/What-Is-LoRa/LoRaWAN-White-Papers

[9] M. Saravanan, A. Das, and V. Iyer, "Smart water grid management using LPWAN IoT technology," in *Proc. Global Internet Things Summit (GIoTS)*, Jun. 2017, pp. 1–6.

[10] J. D. Loftis, S. Katragadda, S. Rhee, and C. Nguyen, "StormSense: A blueprint for coastal flood forecast information & automated alert messaging systems," in *Proc. IEEE Int. Sci. Smart City Oper. Platforms Eng. Partnership Global City Teams Challenge (SCOPE-GCTC)*, Apr. 2018, pp. 12–17.

[11] Semtech Corporation. *LoRa Modulation Basics*. Accessed: Nov. 3, 2018. [Online]. Available: https://www.semtech.com/uploads/documents/an1200.22.pdf

[12] A. Augustin, J. Yi, T. Clausen, and W. M. Townsley, "A study of LoRa: Long range & low power networks for the Internet of Things," *Sensors*, vol. 16, no. 9, p. 1466, 2016.

[13] J. Petajajarvi, K. Mikhaylov, A. Roivainen, T. Hanninen, and M. Pettissalo, "On the coverage of LPWANs: Range evaluation and channel attenuation model for LoRa technology," in *Proc. 14th Int. Conf. ITS Telecommun. (ITST)*, Dec. 2015, pp. 55–59.

[14] F. Adelantado, X. Vilajosana, P. Tuset-Peiro, B. Martinez, J. Melia-Segui, and T. Watteyne, "Understanding the limits of LoRaWAN," *IEEE Commun. Mag.*, vol. 55, no. 9, pp. 34–40, Sep. 2017.

[15] N. Varsier and J. Schwoerer, "Capacity limits of LoRaWAN technology for smart metering applications," in *Proc. IEEE Int. Conf. Commun. (ICC)*, May 2017, pp. 1–6.
[16] R. Piyare, A. L. Murphy, M. Magno, and L. Benini, "On-demand TDMA for energy efficient data collection with LoRa and wake-up receiver," in *Proc. 14th Int. Conf. Wireless Mobile Comput., Netw. Commun. (WiMob)*, Oct. 2018, pp. 1–4.
[17] B. Reynders, Q. Wang, P. Tuset-Peiro, X. Vilajosana, and S. Pollin, "Improving reliability and scalability of lorawans through lightweight scheduling," *IEEE Internet Things J.*, vol. 5, no. 3, pp. 1830–1842, Jun. 2018.
[18] M. Lauridsen, H. Nguyen, B. Vejlgaard, I. Z. Kovacs, P. Mogensen, and M. Sorensen, "Coverage comparison of GPRS, NB-IoT, LoRa, and SigFox in a 7800 km^2 area," in *Proc. IEEE 85th Veh. Technol. Conf. (VTC Spring)*, Jun. 2017, pp. 1–5.
[19] L. Liy, M. C. Vuran, and I. Akyildiz, *Characteristics of Underground Channel for Wireless Underground Sensor Networks*. 2012.
[20] G. Ferre, "Collision and packet loss analysis in a LoRaWAN network," in *Proc. 25th Eur. Signal Process. Conf. (EUSIPCO)*, Aug./Sep. 2017, pp. 2586–2590.
[21] A. Rahmadhani and F. Kuipers, "When LoRaWAN Frames Collide," in *Proc. 12th Int. Workshop Wireless Netw. Testbeds, Exp. Eval. Characterization (WiNTECH)*, New Delhi, India, 2018, pp. 89–97.
[22] H.-C. Lee and K.-H. Ke, "Monitoring of large-area IoT sensors using a LoRa wireless mesh network system: Design and evaluation," *IEEE Trans. Instrum. Meas.*, vol. 67, no. 9, pp. 2177–2187, Sep. 2018.
[23] L. Qiao, Z. Zheng, W. Cui, and L. Wang, "A survey on Wi-Fi HaLow technology for Internet of Things," in *Proc. 2nd IEEE Conf. Energy Internet Energy Syst. Integr. (EI2)*, Oct. 2018, pp. 1–5.
[24] F. Blumensaat, C. Ebi, S. Dicht, J. Rieckermann, and M. Maurer, "Highly distributed long-term monitoring of in-sewer dynamics using low-power radio technology," in *Proc. 12th IWA Specialized Conf. Instrum., Control Automat.*, Québec City, QC, Canada, Jun. 2017. pp. 325–331. [Online]. Available: http://www.ica2017.org/conference-proceedings
[25] Y. Chen, Q. Wang, M. Chang, and A. Terzis, "Ultra-low power time synchronization using passive radio receivers," in *Proc. 10th ACM/IEEE Int. Conf. Inf. Process. Sensor Netw.*, Apr. 2011, pp. 235–245.
[26] EU. *Short Range Devices (SRD) Operating in the Frequency Range 25 MHz to 1000 MHz | Part 1: Technical Characteristics and Methods of Measurement*. 75p. Accessed: Aug. 31, 2018. Available: https://www.etsi.org/deliver/etsi_en/300200_300299/30022001/03.01.01_30/en_30022001v030101v.pdf
[27] D. Piester, P. Hetzel, and A. Bauch, "Zeit-und Normalfrequenzverbreitung mit DCF77," *PTB-Mitteilungen*, vol. 114, no. 4, p. 24, 2004.
[28] HKW-Elektronik. *FUM DCF-U | Funkuhrmodul DCF-U*. Accessed: Aug. 31, 2018. [Online]. Available: https://www.hkw-shop.de/out/media/FMD01031R_FUM_DCF-U_DD.pdf
[29] Delano. *FGPMMOPA6H GPS Standalone Module Data Sheet*. 37p. Accessed: Aug. 29, 2018. [Online]. Available: https://cdn-shop.adafruit.com/datasheets/GlobalTop-FGPMMOPA6H-Datasheet-V0A.pdf
[30] IMST-GmbH. *WiMOD iM880B Datasheet*. 24p. Accessed: Aug. 29, 2018. Available: https://wireless-solutions.de/downloads/Radio-Modules/iM880B/General_Information/iM880B_Datasheet_V1_5.pdf
[31] Semtech Corporation. (2017). *Datasheet-SX1272/73-860 MHz to 1020 MHz Low Power Long Range Transceiver*. [Online]. Available: https://www.semtech.com/uploads/documents/sx1272.pdf
[32] IMST-GmbH. *WiMOD LoRaWAN EndNode Modem HCI Specification*. 90p. Accessed: Aug. 29, 2018. [Online]. Available: https://wireless-solutions.de/downloads/Radio-Modules/iM880B/WiMOD_LoRaWAN/WiMOD_LoRaWAN_EndNode_Modem_HCI_Spec_V1_22.pdf
[33] (2018). *The FreeRTOSTM Project Website*. [Online]. Available: http://www.freertos.org
[34] STMicroelectronics. (Apr. 2018). *RM0351-Reference Manual for STM32L4×5 and STM32L4×6 advanced Arm-based 32-Bit MCUs*. 1881p. Accessed: Aug. 31, 2018. Available: https://www.st.com/resource/en/reference_manual/dm00083560.pdf

CHRISTIAN EBI received the Dipl.Ing. FH (B.S.) degree in electrical engineering from HSR or the University of Applied Sciences, Rapperswil, Switzerland, in 1996.

He joined the Swiss Federal Institute of Aquatic Science and Technology, Eawag, Dübendorf, Switzerland, in 2015, as a Specialist for sensor networks and technology. He was also with industry for 19 years as a Research and Development Engineer and Project Manager. During his time in the industry, he initially focused on frequency synthesis methods, RF systems and sensors for analytical instruments, and later on low-power and embedded systems. His current interests include long-range communication, low-power data acquisition, and environmental monitoring.

FABIAN SCHALTEGGER received the B.Sc. degree in electrical engineering from the Zurich University of Applied Sciences (ZHAW), Winterthur, Switzerland, in 2015, where he is currently pursuing the M.Sc. degree. Since 2015, he has been as a Scientific Assistant with the Institute of Embedded Systems (ZHAW). His work focuses on enabling technologies for the Internet of Things, especially on low-power wireless sensor networks in conjunction with LoRaWAN.

ANDREAS RÜST received the master's degree in electrical engineering from the Federal Institute of Technology, Zurich, in 1991. He is currently a Professor in the Internet of Things with the Zurich University of Applied Sciences (ZHAW), Winterthur, Switzerland. He has 20 years of industry experience in the fields of microcontroller chip design and the development of SHDSL modems. He currently leads a research area with the Institute of Embedded Systems. Over the last eight years, his research was focusing on scalable and secure low-power wireless networks.

FRANK BLUMENSAAT received a Diploma degree in urban water management and later a Ph.D. degree in environmental engineering from the Technical University of Dresden, Germany. He is currently a Senior Researcher with the Swiss Federal Institute of Aquatic Science and Technology, Eawag, and a Senior Lecturer with the Swiss Federal Institute of Technology, ETH Zurich. He has 15 years of experience in urban water resources management, and specializing in monitoring and modelling urban drainage systems. At Eawag, his current research interests include exploring novel data collection techniques and emerging data sources to enable a more efficient urban water management.